Jacob C. Snyder
Department of Mechanical
and Nuclear Engineering,
Penn State University,
START Lab,
3127 Research Drive,
State College, PA 16801
e-mail: jacob.snyder@psu.edu

Curtis K. Stimpson
Department of Mechanical
and Nuclear Engineering,
Penn State University,
START Lab,
3127 Research Drive,
State College, PA 16801
e-mail: curtis.stimpson@psu.edu

Karen A. Thole
Department of Mechanical
and Nuclear Engineering,
Penn State University,
136 Reber Building,
University Park, PA 16802
e-mail: kthole@psu.edu

Dominic J. Mongillo
Pratt and Whitney,
400 Main Street,
East Hartford, CT 06118

Build Direction Effects on Microchannel Tolerance and Surface Roughness

With the advance of additive manufacturing (AM) processes, complex designs can be created with engineering metals. One specific advantage of this greater design space is the ability to create small internal channels and passageways for cooling high heat flux or temperature applications such as electronics and gas turbine airfoils. These applications can have complex shapes, which when coupled with the required small channel sizes, make traditional finishing processes a challenge for additively manufactured parts. Therefore, it is desirable for designers to be able to use AM parts with small internal channels that are as-built. To achieve this goal, however, designers must know how the AM process affects internal channel tolerances and roughness levels, since both impact the amount of cooling that can be achieved in actual applications. In this study, the direct metal laser sintering (DMLS) process, more generically referred to as selective laser melting (SLM), was used to additively manufacture test coupons. The AM build direction was varied to study its effect on small microsized, circular channels. Specifically, X-ray computed tomography (CT-scan) was used to nondestructively inspect the interior of the test coupons. Using the data from the CT-scans, internal surface roughness, geometric tolerances, and deviations from the computer-aided design (CAD) model were calculated. In comparing the data, significant differences were seen between the three different build directions.
[DOI: 10.1115/1.4031071]

Introduction

As the capabilities of AM continue to expand, the applicability of AM to production parts increases. Specifically, the advancement of powder metal AM processes, such as DMLS, has allowed metal components to be manufactured with geometries too complicated for subtractive manufacturing. This capability to manufacture complex parts has been commonly demonstrated using topology optimization and bio-inspired designs. There are also significant advantages that AM brings to internal features such as the ability to manufacture complicated flow paths and internal features which can enhance heat transfer and satisfy geometric constraints. The advantages of AM can lead to a paradigm shift in cooling designs for the electronics and aerospace industries, where components often have significant heat loads and complicated geometry. A specific application of AM in the aerospace industry is the gas turbine engine. Gas turbine engines have intricate cooling designs to remove heat from critical parts, such as turbine airfoils, through the use of relatively cooler compressor air that bypasses the combustor. Removing this heat is essential to the longevity of the engine: an increase in metal temperature of 4 °C can decrease the component's life by one half [1].

The small scale of components in the aerospace and electronics industries complicates the task of removing heat. Decreasing the size and number of the cooling channels generally improves the cooling efficiency for a variety of reasons. However, reducing the feature size of cooling channels complicates the task of subtractive manufacturing. AM is well suited to producing intricate microchannel designs. In these intricate microchannels operating under a given pressure ratio, accurate dimensions with small tolerances are essential to ensure predictable flowrates. The complex shapes desired for cooling efficiency, coupled with the small channel sizes, make utilizing traditional finishing processes to control part tolerances and surface roughness a challenge. To reduce costs and time, it is desirable to use these complex small channels as manufactured rather than treating them with elaborate postmanufacturing methods.

While there are many process variables to study, build direction has a strong effect on all additively manufactured parts. Different build directions for a particular part can affect manufacturing time and cost. The goal of this study, therefore, was to evaluate the effect of build direction on the quality of microchannels.

This paper begins by reviewing relevant AM works in the literature. Next, descriptions of the methods are given for manufacturing and analysis. Finally, results are presented for channel tolerances and surface roughness, followed by conclusions.

Literature Review

In recent years, there has been much work reported in public literature related to AM. With the advance of metal based AM, a majority of research has been focused on material qualification related to microstructure and mechanical properties. While this research has been essential to developing the processes, the current research goal is to examine how the process affects the final quality of AM parts. In this area, researchers have characterized surface roughness and dimensional errors on the exterior of parts larger than the coupons examined in this study.

Contributed by the Design for Manufacturing Committee of ASME for publication in the Journal of Mechanical Design. Manuscript received March 4, 2015; final manuscript received July 7, 2015; published online October 12, 2015. Assoc. Editor: Christopher Williams.

One area of focus has been the build direction effect on external surface roughness. Strano et al. [2] studied various angled surfaces of 316 L steel parts made with SLM. They found that the roughness was around 15 μm for all angles between horizontal and 45 deg, and decreased as the angle approached the vertical. Ventola et al. [3], Simonelli et al. [4], and Delgado et al. [5] also found that build direction strongly affects surface roughness, with values dramatically increasing at angled build directions. Cooper et al. [6] looked at angle effects by ordering different surfaces of a single part by roughness values. Horizontal upward-facing surfaces had the lowest surface roughness, followed by sloped upward-facing surfaces, while sloped downward-facing surfaces had the highest surface roughness.

Delgado et al. [5], along with other researchers [7–9], investigated the effects of DMLS process parameters, such as layer thickness, laser scan speed, laser power, and hatching distance on the surface roughness of DMLS parts. While these parameters were found to have some effect on the roughness, the build direction still had the strongest effect. Overall, common roughness values found in the literature range between about $5 < R_a < 50$ μm and are strong functions of machine parameters and build direction [2–11].

In addition to surface roughness, the dimensional tolerance of additively manufactured parts has been studied. Early studies looked at optimizing the build direction to minimize dimensional errors. Masood et al. [12,13] developed a generic model based on minimizing volumetric error due to the stair stepping effect of AM. Arni and Gupta [14] also worked on a method to minimize the stair stepping effect where flatness tolerance was used as the metric to evaluate the build orientations. Paul and Anand [15] performed a similar study where cylindricity error was characterized as a function of build direction. These studies, however, were all analytical and based purely on geometric calculations.

Work has also been done to try to predict dimensional errors for a given part. Paul and Anand [16] modeled the shrinkage of powder based AM processes. Using a simple analysis of material density changes, the model was used to predict form errors such as cylindricity and flatness. This model was refined in a later study by Paul et al. [17] to include a finite element analysis to correctly capture thermal distortion effects along with volumetric shrinkage. Again, these studies were purely analytical and did not include any experimental validation. Furthermore, these studies did not take into account the complex interactions of process parameters in metal AM processes.

To understand some of these complex interactions, experimental studies have been performed evaluating dimensional tolerances and shrinkage effects of DMLS samples [6,11,18]. Of high relevance to the current study was the finding by Ning et al. [18] that smaller geometries were more susceptible to absolute dimensional error due to shrinkage.

One of the few studies to experimentally examine the build direction effects on part tolerance was done by Delgado et al. [5]. They studied the effect of build direction on surface roughness and dimensional tolerance for stainless steel DMLS parts. While this study only investigated two build directions, the authors found that the build direction had a much larger effect on surface roughness and dimensional tolerance than any other process parameter. Tensile test specimens were manufactured and compared to the design intent, with deviations as high as 23.5% for certain dimensions. Other studies [4,19] have investigated the effect of build direction on mechanical properties of SLM and DMLS parts. However, no build direction studies have examined the effects on internal channel tolerances.

Despite the number of studies in the literature focused on optimal part orientation, few have experimentally studied the build direction effects on final part quality for metal processes. The few that have studied build direction effects, worked to characterize material quality and tolerance of large external features. Currently, there is no work in the literature focused on small microscale channels. This study seeks to provide critical information to designers on how different builds directions affect the quality of small internal channels.

Coupon Design and Manufacturing

To examine the build direction effects on the internal channel quality, a number of test coupons were designed and manufactured in-house using state-of-the-art DMLS equipment. As shown in Fig. 1, the overall dimensions of the coupon were 25.4 mm long, 25.4 mm wide, and 3.05 mm high. Fifteen circular microchannels with a 0.508 mm diameter were designed to run through the center of the coupon spaced 2.5 diameters apart. Flanges on the ends of the coupon interfaced with a test facility for separate experimental studies [20,21]. The powdered metal used to manufacture the coupons was Inconel 718.

The coupon geometry was manufactured in three different build directions shown in Figs. 2(*a*)–2(*c*): vertical, horizontal, and diagonal. All of the coupons were manufactured in a single build session. The position of the channel axes relative to the build plate defined each build direction. The channel axes were perpendicular to the build plate in the vertical build direction, parallel to the build plate in the horizontal build direction, and at a 45 deg angle to the build plate in the diagonal build direction. These directions were chosen to evaluate the extremes of the layer-by-layer nature of the additive process. In the vertical orientation, channel surfaces were formed by the edges of each layer. In the horizontal orientation, channel surfaces were made up of: edges of layers, tops of layers, and bottoms of layers. Finally, surfaces in the 45 deg orientation were made up of layer edges in the form of "stair steps," caused by the addition of subsequent layers.

Support structures were necessary to successfully manufacture the coupons. Most AM methods require structures to support overhanging features so they do not collapse, and to anchor the part to the build plate to minimize warping. Specific to the DMLS process with Inconel 718, the minimum recommended unsupported angle is 40 deg. Any surface of the test coupons, which was less than 40 deg to horizontal, required supports. Using these criteria, the upper surface of the horizontal cylindrical channels should

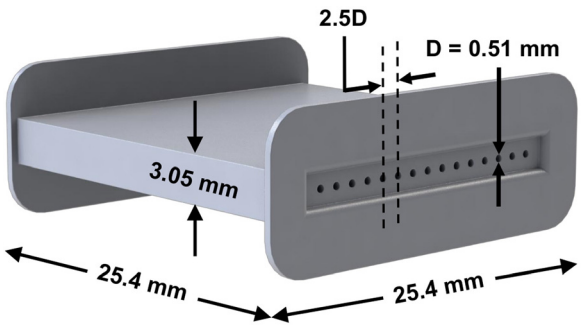

Fig. 1 Designed dimensions, shape, and channel spacing of the test coupons

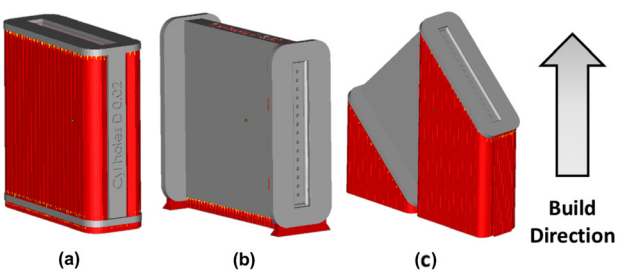

Fig. 2 Coupon orientation and support structures (shown in red/darker gray) for the (*a*) vertical, (*b*) horizontal, and (*c*) diagonal build directions

Table 1 Build parameters used to manufacture all test coupons

Parameter	Value
Material setting	IN718 040 performance
Material scaling X	0.045%
Material scaling Y	0.16%
Beam offset	0.11 mm
Layer thickness	0.04 mm
Nominal powder size	0.03 mm

have had supports; however, it would be difficult to remove these supports after the build was completed. The horizontal surfaces of the channels were intentionally unsupported to replicate situations, where internal features require supports but cannot be accessed for support removal.

The support structures used to build the coupons are shown in Fig. 2. In addition to using supports for surfaces angled at 40 deg or less, supports were placed on other features, such as the coupon flanges, to prevent distortion by anchoring the part to the build plate. For this study, the support structures were generated using a commercial stereolithography (STL) file editing and build preparation software.

A state of the art DMLS machine was used to manufacture the test coupons using the machine parameters given in Table 1. Prior to building the coupons, a qualification block was built out of Inconel 718 to calculate the material scaling parameters and beam offset. These calculations were carried out per the manufacturer's specifications [22]; no advanced process parameter development was used for this study. Since the goal of this work was to investigate build direction, the process parameters were kept constant across all coupons. The total time for the build was 53 hrs, which included a total of 76 coupons. Note that not all coupons built are presented in this study.

Once the coupons were completed, residual stresses generated during the manufacturing process were removed with a heat treatment process. Removing the residual stresses was essential to prevent distortion. After the heat treatment, wire electrical discharge machining (EDM) was used to cut the coupons from the build plate. Manual machining and hand tools were then used to remove any remaining support material.

Measurement Methodology

Since the goal of this particular study was to investigate the quality of the microchannels in the test coupons, advanced inspection techniques were developed using CT scans. An industrial CT scanner was used to scan each test coupon, while a companion software package generated a 3D reconstruction of the coupon from the raw scan data. This 3D reconstruction had a resolution (i.e., voxel size) of 35 μm. To perform quantitative analyses on the data, the surface location for each coupon was determined by examining the gradient of grayscale values in the CT scan images. By using a commercial imaging software, which made a local comparison of these gray values, accuracies in the surface determination of 1/10th of the voxel size can be achieved [23]. Thus, the surface determined with the CT scan was accurate to within 3.5 μm.

To compare the interior surfaces of the microchannels directly to the CAD model from which it was manufactured, an STL model of the test coupon was loaded into the commercial imaging software [24]. The STL model was matched to the CT scan surface using a best fit algorithm. With the STL model registered correctly, the difference between the CAD model and manufactured part was calculated.

The determined surface of the part was also exported as a three-dimensional point cloud for further analysis. The number of points defining each channel was monitored to ensure that the spatial resolution of the point cloud matched the expected spatial resolution of the surface determination. In most cases, the point cloud was nominally 500 K points per channel. An in-house code was used to analyze the point clouds defining each channel separately.

Tolerance Analysis Method. The point clouds for each channel were used to calculate four different tolerance measures: maximum inscribed diameter, effective diameter, total runout, concentricity, and circularity. Maximum inscribed diameter and effective diameter are two ways to measure the size of the microchannels, while total runout, concentricity, and circularity are common geometric dimensioning and tolerancing measures to control the shapes of cylindrical features. To calculate these variables, the point cloud was divided into 500 equal slices in the axial direction of the 25.4 mm long microchannels. All the points within each slice were then considered to lie in the same plane.

The maximum inscribed diameter represents the largest pin gauge that could fit through any given cross section of the channel. This diameter was calculated by inscribing a circle to each planar dataset. The reported value for each channel is the smallest of the inscribed circles of all of the 500 slices.

Effective diameter is a way to represent a diameter for a noncircular channel using its cross-sectional area, A_c, and perimeter, P. To determine A_c and P, each of the 500 slices was split into upper and lower halves. A polynomial curve was then fit to the data on each half, allowing the freeform shape of the channel to be represented by two mathematical functions: one for the upper and one for the lower halves. These functions were then used to determine the total perimeter and area of each slice. An average was taken over all 500 slices, and the result was used in Eq. (1) to calculate the effective diameter

$$D_{\text{eff}} = 4\frac{\bar{A}_c}{\bar{P}} \tag{1}$$

Concentricity was determined by fitting a circle to the planar data in each of the 500 slices. Next, the centers of all of these circles were compared to one another. The concentricity tolerance reported is the largest distance between the center points of any two slices. Concentricity is defined visually in Fig. 3(*a*).

Circularity, a measure of the roundness of any given cross section was measured by circumscribing the data for each planar dataset. The radius of the circle inscribing the data was then subtracted from the radius of the circumscribed circle. This gave the size of the annular region containing all the data points for each slice. The circularity reported is the largest of these annular regions for each channel. Circularity is defined visually in Fig. 3(*b*).

Calculating the total runout required establishing an axis to "rotate" the channel about. The direction of this axis was determined by performing a principle component analysis on the data for the entire channel. This vector defining the axis direction was then centered on the mean of the data to create the channel axis. With the channel axis determined, the total runout was then determined by calculating the difference between the maximum and minimum radial distances of the data points from the channel

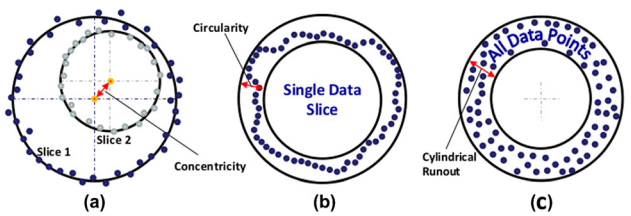

Fig. 3 Geometric tolerance definitions for (*a*) concentricity, (*b*) circularity, and (*c*) total runout

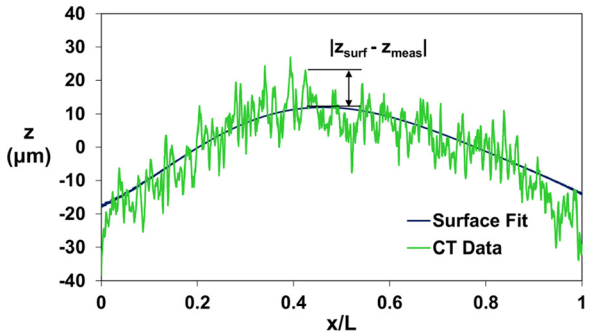

Fig. 4 A slice taken along the channel axis showing the roughness features and surface fit for one plane of the vertically built channel surface

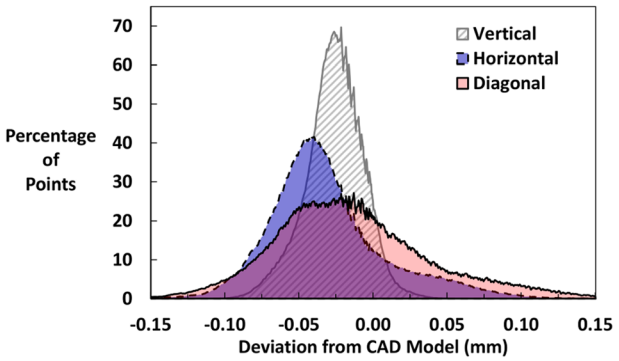

Fig. 6 Distribution of the difference between the coupon surface points and the CAD model for the three different build directions

axis. The value reported is the average of the largest differences for each channel. Total runout is defined visually in Fig. 3(*c*).

Roughness Analysis Method. In addition to calculating geometric tolerances, the point clouds from the CT scans were used to nondestructively measure the internal surface roughness of the channels. To measure surface roughness, a reference was needed to determine the heights of the roughness features. Since these channel surfaces were not regular, a 3D surface was fit to the data to be used as the reference. The *R*-square values of these surface fits were low, between 0.53 and 0.64, since the surface fit was used to represent a mean surface. Figure 4 shows an example of this method from the vertically built coupon. Taking a slice along the channel axis shows how the 3D surface fits to one plane of the roughness data. This surface fit removed the waviness and irregular curvature from the data, leaving only roughness features. An arithmetic mean roughness, R_a, was then calculated by averaging the distance between the reference surface and all the individual data points, shown in the below equation

$$R_a = \frac{1}{n}\sum_{i=1}^{n}|z_{surf} - z_{meas}| \tag{2}$$

Due to the resolution of the CT scanner, some roughness features were not captured in the CT scan. Specifically, features that were smaller than the voxel size were washed out in the scan. To examine the effect of the limited CT scan resolution on the roughness measurement, a comparison was made to measurements from a state-of-the-art optical profilometer. Measurements with a scan length of 2.6 mm were taken from the interior and exterior of the coupon to generate a large sample size. To make interior optical profilometer measurements, a sacrificial test coupon was cut open to expose the channel surfaces. Shown in Fig. 5 are contour plots of the same DMLS surface as measured by a CT scan and by an optical profilometer. The CT scan captured large roughness features but failed to resolve the entire surface morphology captured by the optical profilometer. Quantitatively, the CT scan roughness measurements were statistically different from the optical profilometry measurements of identical surfaces. Moreover, the CT scan consistently underpredicted the result from the optical profilometer. Despite this difference, the CT scan measurements are preferable since they can be completed nondestructively. The roughness results presented in the paper, therefore, serve as estimates to the actual surface roughness but still allow comparisons among the different build directions.

Channel Tolerances

To understand the tolerance of each coupon as a whole, the CT scan was first compared to the CAD model. This comparison was made by calculating the difference between the CT scan surface and the CAD model surface, relative to the normal at the CAD surface. Therefore, a positive deviation indicates that the CT scan surface lies outside the CAD surface, in the direction of the normal. As presented in Fig. 6, each build direction has a different deviation distribution for the coupon's interior surfaces. However, each of the three peaks is similarly centered on a negative deviation value. This offset of the peaks indicates that for all three build directions, the channels were built slightly larger than specified by the CAD model. Overcompensating for material shrinkage is most likely responsible for the slightly larger channels.

Material shrinkage is a result of two factors: the lower bulk density of the powder compared to the solid material and the contraction of the material as the part cools. These effects are inherent to metal AM and are addressed in the DMLS manufacturer's instructions for operating the machine [22]. These instructions define a method to determine the material scaling parameter, using a qualification block built with the same machine and material.

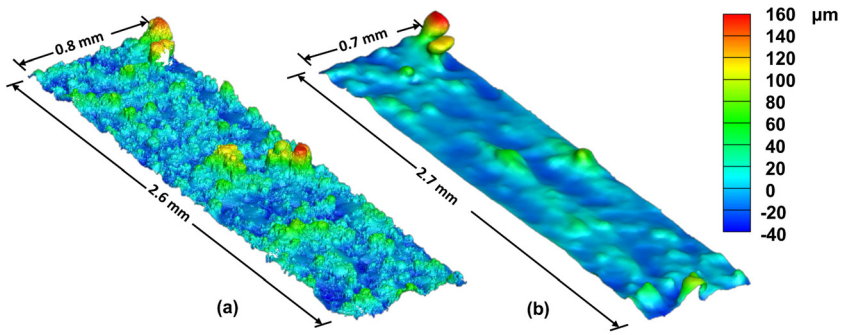

Fig. 5 Comparison of surface roughness contours from (*a*) an optical profilometer and (*b*) a CT scanner showing features missing in CT scan data

Table 2 Geometric tolerance data calculated from channel CT scans

	Vertical		Horizontal		Diagonal	
	Ave	σ	Ave	σ	Ave	σ
Inscribed D (mm)	0.499	0.005	0.440	0.010	0.438	0.007
Effective D (mm)	0.554	0.012	0.532	0.005	0.532	0.005
Total runout (mm)	0.134	0.015	0.221	0.022	0.225	0.032
Concentricity (mm)	0.026	0.007	0.113	0.014	0.114	0.013
Circularity (mm)	0.092	0.012	0.193	0.075	0.219	0.084
Surface roughness R_a (μm)	8.4		16.1		16.3	

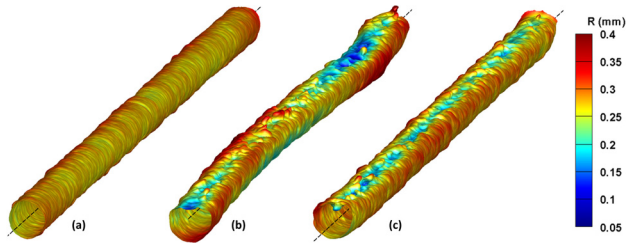

Fig. 7 Three-dimensional surfaces representing the internal channel topology of a single channel for the (*a*) vertical, (*b*) horizontal, and (*c*) diagonal build directions

Because the part used to determine the scaling parameter was not the coupon from this study, the scaling was not tuned to the specific shrinkage behavior of this geometry. Modeling to predict the shrinkage and generate these material scaling parameters is an area of much needed ongoing research [25,26].

Also shown in Fig. 6 are the differences in surface deviation between the three different build directions. The vertical build direction had the narrowest distribution, indicating the surface deviated from the CAD model more uniformly than the diagonal and horizontal build directions. To understand this difference, the 2D geometry of the layers used to construct the channels was examined. The geometry of each layer in the vertical build direction was identical, while the geometry of the layers in the diagonal and horizontal build directions was dependent on the z location of the layer relative to the build plate. Because the layers were identical in the vertical build direction, the same dimensional errors were repeated, generating the narrower deviation distribution shown in Fig. 6.

Additional insight into these dimensional errors can be gained by examining the diameters of the channels. As described above, two different measures of diameter were used: maximum inscribed and effective. The averages of these measures across all channels are presented in Table 2. Looking at the maximum inscribed diameter, the vertical build direction resulted in a channel diameter only 3% smaller than the design intent. The horizontal and diagonal build directions, on the other hand, had maximum inscribed diameters that were 18% and 16% smaller than the design intent, respectively. These deviations from the design intent are similar to those seen in DMLS samples studied by Delgado et al. [5]. When looking at the effective diameter, however, the opposite trend is seen. All of the build directions resulted in an effective diameter larger than the design intent, with the horizontal and diagonal directions coming closer to the design intent than the vertical direction. The lack of agreement between trends can be understood by examining the shape of the channels.

Shown in Fig. 7 are 3D surfaces representing one channel from each build direction. In the horizontal and diagonal build directions, the top surface of the channel is deformed. The irregular shape of the channel limits the size of the perfect circle that could fit inside of each cross-sectional slice, decreasing the inscribed diameter. Alternatively, the overall cross-sectional area and perimeter of the channel were not affected as much by the deformation. Therefore, the effective diameter is slightly larger than the design intent because of the nonoptimized material shrinkage parameter discussed previously.

To further analyze the deformations in channel shape, measures of geometric tolerance were also calculated from the CT scan data. Referring to Table 2, the vertical build direction had the smallest circularity tolerance. In other words, the vertical build direction produced the channel shape closest to a circle. The other build directions generated noncircular channel shapes, and therefore, larger circularity tolerances. These circularity tolerances explain the differences in inscribed diameter discussed previously.

The vertical build direction had the smallest average concentricity tolerance, indicating that this build direction yielded channels with the best aligned cross sections. The alignment of the cross sections can be confirmed visually in Fig. 8. Axial slices were made in five locations along a channel from each build direction. Slices from the vertically built channel lie nearly perfectly on top of each other, while slices from the other two channels show variability along their length. The small concentricity tolerance of the vertical build direction can be attributed to the consistent shape of the build layers. Since each slice had the same geometry during the build, the solidification and cooling of each layer was similar. This consistency helped to produce channels where each cross section was correctly aligned with the preceding layer.

Examining the total runout tolerance was another way to evaluate the deformation of the channels. Similar to the other tolerance measures, the vertical channel had the lowest runout. Interestingly, the horizontal and diagonal build directions had comparable runout tolerances. Lack of support material explains this poor tolerance in the horizontal coupon. However, this does not explain the deformation in the diagonal coupon, since the upper surface should have been self-supporting. The large deformations, and thus high runout tolerance, of the diagonally built channels are

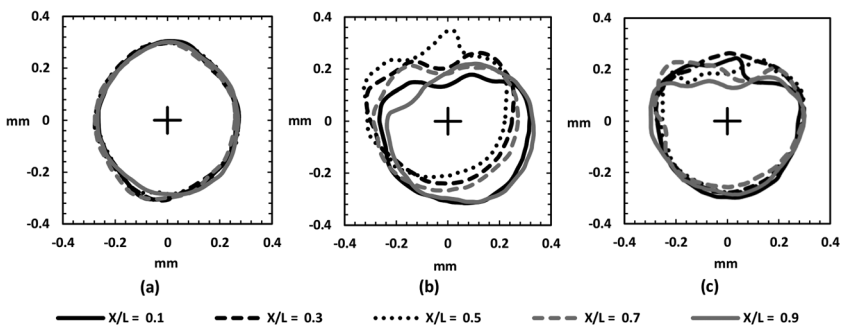

Fig. 8 Axial slices at various streamwise locations of (*a*) vertically, (*b*) horizontally, and (*c*) diagonally built channels

instead explained by the size of the laser melt pool. Although its size is dependent on the laser power and scan speed, a typical melt pool penetrates further into the part than the current layer [27,28]. When building the upper surface of the channel in the diagonal build direction, the heat from the laser penetrated deeper than the current layer, melting some of the powder inside the channel. This overmelting generated the globular features shown in Fig. 7. In addition, these defects compounded the distortion seen in the upper channel surface by hindering the creation of subsequent layers [29].

Conduction differences during the build could have exacerbated the deformations and inconsistencies seen with the different build directions. Given the support structures shown in Fig. 2, the heat from the melt pool must conduct to the build plate through different paths in each build direction. In the diagonal build direction, there are no supports on the downward facing exterior surface. Therefore, all of the heat must conduct to the plate through the small amount of support structure at the bottom of the flange. This small connection to the build plate could have slowed the rate of solidification each layer, and thus impeded the ability to hold a tight tolerance on the overhanging upper surface of the channel.

Channel Roughness

Surface roughness on the interior of the channels was also examined for the three different build directions. Referring to Table 2, the vertically built channels had the lowest internal surface roughness of all the test coupons. This low R_a value can be attributed to the lack of downward facing surfaces in the channel. As reported in the literature [6,20], downward facing surfaces are rougher than upward facing surfaces, with vertical surfaces lying somewhere in between. This difference has to do with the layer-by-layer nature of AM. Upward-facing surfaces are the smoothest since the laser beam melts that surface directly. Downward-facing surfaces are rough due to the unsintered powder that the surfaces are built upon. Powder can fuse to the layer created above it, resulting in small ball-like features on the surface. These features can be seen in the optical profilometry image in Fig. 5(*a*). Finally, vertical surfaces have medium roughness values in between upward-facing and downward-facing since they are composed of the edges of all of the layers. These layer edges can be seen in the vertically built channel surfaces shown in Fig. 7(*a*). As seen by Strano et al. [2], the horizontally and diagonally built channels have similar roughness values. Both channels have an upward facing surface and a downward facing surface, which explains the similarity in roughness.

Roughness levels found for all three coupons were similar to those reported for the DMLS process with various materials [2–11]. These roughness levels are more than double those typically seen with a machining, EDM, or investment casting process [30]. Therefore, using DMLS to create small channels resulted in internal surfaces rougher than traditional methods, regardless of the DMLS build direction. At the small scale of these channels, these high roughness levels are significant.

Conclusions

Coupons for evaluating dimensional tolerance and surface roughness of microscale channels were fabricated out of Inconel 718 using three different build directions. These coupons were CT scanned to generate data for further analysis. Codes developed in-house were then used to calculate the internal dimensions, geometric tolerances, and surface roughness of the channels. Despite the CT scanner's lack of resolution for surface roughness measurements, the data allowed comparisons between the build directions and visualization of the large internal roughness features without destroying the coupon.

In general, the vertical build direction produced the highest quality channels. Tolerance values of total runout, concentricity, and circularity were lowest for the vertically built channels, while the maximum inscribed diameter was closest to the design intent. In addition, the vertical build direction resulted in the lowest internal surface roughness of all of the coupons tested.

Despite a difference of 45 deg between the horizontal and diagonal build directions, these directions produced channels with similar diameters, tolerances, and surface roughness. Therefore, designers must be cautious if a design requires a channel to be built 45 deg or lower relative to the build plate. At the microchannel scale, the impact of roughness features and geometric deviations can be severe. With few finishing processes well suited to this small scale, the high roughness and geometric deviations must be accounted for from the beginning of the design process.

Acknowledgment

Technical assistance and the equipment used for manufacturing the test coupons and performing CT scans were provided by CIMP-3D. Technical assistance and equipment used for the optical profilometry measurements were provided by the Materials Characterization Lab at Penn State University. The support of both organizations was critical to the success of this project. Their efforts are much appreciated. This research was funded by Pratt & Whitney (P&W). Their financial support was greatly appreciated.

Nomenclature

A_c = cross-sectional area of a channel
L = length of the channel
n = number of points in the 3D point cloud for a given channel
P = perimeter of a channel
R_a = arithmetic mean roughness
x = x-coordinate of the build envelope
X = axial position along the channel
y = y-coordinate of the build envelope
z = z-coordinate of the build envelope
Z_{meas} = height of the measured CT scan surface in the roughness reference frame
Z_{surf} = height of the polynomial surface fit in the roughness reference frame

References

[1] Han, J. C., Dutta, S., and Ekkad, S., 2000, *Gas Turbine Heat Transfer and Cooling*, Taylor and Francis, New York.
[2] Strano, G., Hao, L., Everson, R. M., and Evans, K. E., 2013, "Surface Roughness Analysis, Modelling and Prediction in Selective Laser Melting," J. Mater. Process. Technol., **213**(4), pp. 589–597.
[3] Ventola, L., Robotti, F., Dialameh, M., Calignano, F., Manfredi, D., Chiavazzo, E., and Asinari, P., 2014, "Rough Surfaces With Enhanced Heat Transfer for Electronics Cooling by Direct Metal Laser Sintering," Int. J. Heat Mass Transf., **75**, pp. 58–74.
[4] Simonelli, M., Tse, Y. Y., and Tuck, C., 2014, "Effect of the Build Orientation on the Mechanical Properties and Fracture Modes of SLM Ti–6Al–4V," Mater. Sci. Eng. A, **616**, pp. 1–11.
[5] Delgado, J., Ciurana, J., and Rodríguez, C. A., 2012, "Influence of Process Parameters on Part Quality and Mechanical Properties for DMLS and SLM With Iron-Based Materials," Int. J. Adv. Manuf. Technol., **60**(5–8), pp. 601–610.
[6] Cooper, D. E., Stanford, M., Kibble, K. A., and Gibbons, G. J., 2012, "Additive Manufacturing for Product Improvement at Red Bull Technology," Mater. Des., **41**, pp. 226–230.
[7] Song, Y.-A., and Koenig, W., 1997, "Experimental Study of the Basic Process Mechanism for Direct Selective Laser Sintering of Low-Melting Metallic Powder," CIRP Ann.—Manuf. Technol., **46**(1), pp. 127–130.
[8] Calignano, F., Manfredi, D., Ambrosio, E. P., Iuliano, L., and Fino, P., 2013, "Influence of Process Parameters on Surface Roughness of Aluminum Parts Produced by DMLS," Int. J. Adv. Manuf. Technol., **67**(9–12), pp. 2743–2751.
[9] Senthilkumaran, K., Pandey, P. M., and Rao, P. V. M., 2009, "Influence of Building Strategies on the Accuracy of Parts in Selective Laser Sintering," Mater. Des., **30**(8), pp. 2946–2954.
[10] Simchi, A., Petzoldt, F., and Pohl, H., 2003, "On the Development of Direct Metal Laser Sintering for Rapid Tooling," J. Mater. Process. Technol., **141**(3), pp. 319–328.
[11] Khaing, M. W., Fuh, J. Y. H., and Lu, L., 2001, "Direct Metal Laser Sintering for Rapid Tooling: Processing and Characterisation of EOS Part," J. Mater. Process. Technol., **113**(1–3), pp. 269–272.

[12] Masood, S. H., Rattanawong, W., and Iovenitti, P., 2003, "A Generic Algorithm for a Best Part Orientation System for Complex Parts in Rapid Prototyping," J. Mater. Process. Technol., **139**(1–3), pp. 110–116.
[13] Masood, S. H., and Rattanawong, W., 2002, "A Generic Part Orientation System Based on Volumetric Error in Rapid Prototyping," Int. J. Adv. Manuf. Technol., **19**(3), pp. 209–216.
[14] Arni, R., and Gupta, S., 2001, "Manufacturability Analysis of Flatness Tolerances in Solid Freeform Fabrication," ASME J. Mech. Des., **123**(1), pp. 148–156.
[15] Paul, R., and Anand, S., 2011, "Optimal Part Orientation in Rapid Manufacturing Process for Achieving Geometric Tolerances," J. Manuf. Syst., **30**(4), pp. 214–222.
[16] Paul, R., and Anand, S., 2013, "Material Shrinkage Modeling and Form Error Prediction in Additive Manufacturing Processes," NAMRI/SME, pp. 515–525.
[17] Paul, R., Anand, S., and Gerner, F., 2014, "Effect of Thermal Deformation on Part Errors in Metal Powder Based Additive Manufacturing Processes," ASME J. Manuf. Sci. Eng., **136**(3), p. 031009.
[18] Ning, Y., Wong, Y. S., Fuh, J. Y. H., and Loh, H. T., 2006, "An Approach to Minimize Build Errors in Direct Metal Laser Sintering," IEEE Trans. Autom. Sci. Eng., **3**(1), pp. 73–80.
[19] Manfredi, D., Calignano, F., Krishnan, M., Canali, R., Ambrosio, E. P., and Atzeni, E., 2013, "From Powders to Dense Metal Parts: Characterization of a Commercial AlSiMg Alloy Processed Through Direct Metal Laser Sintering," Materials, **6**(3), pp. 856–869.
[20] Stimpson, C. K., Snyder, J. C., and Thole, K. A., 2015, "Roughness Effects on Flow and Heat Transfer for Additively Manufactured Channels," ASME Paper No. GT2015-43940.
[21] Snyder, J. C., Stimpson, C. K., and Thole, K. A., 2015, "Build Direction Effects on Additively Manufactured Channels," ASME Paper No. GT2015-43935.
[22] EOS GmbH, Basic Training EOSINT M 280.
[23] Becker, B., Maier, D., and Reinhart, C., 2012, "Computer Tomography Has Arrived in Automated Inspection Processes, Combining Material and Geometry Analyses," 18th World Conference on Non-Destructive Testing, Durban, South Africa, Apr. 16–20.
[24] VG Studio MAX, Vers. 2.2, Volume Graphics GmbH, Heidelberg, Germany.
[25] Zhu, H. H., Lu, L., and Fuh, J. Y. H., 2006, "Study on Shrinkage Behaviour of Direct Laser Sintering Metallic Powder," Proc. Inst. Mech. Eng. Part B, **220**(2), pp. 183–190.
[26] Raghunath, N., and Pandey, P. M., 2007, "Improving Accuracy Through Shrinkage Modelling by Using Taguchi Method in Selective Laser Sintering," Int. J. Mach. Tools Manuf., **47**(6), pp. 985–995.
[27] Louvis, E., Fox, P., and Sutcliffe, C. J., 2011, "Selective Laser Melting of Aluminium Components," J. Mater. Process. Technol., **211**(2), pp. 275–284.
[28] Verhaeghe, F., Craeghs, T., Heulens, J., and Pandelaers, L., 2009, "A Pragmatic Model for Selective Laser Melting With Evaporation," Acta Mater., **57**(20), pp. 6006–6012.
[29] Olakanmi, E. O., 2013, "Selective Laser Sintering/Melting (SLS/SLM) of Pure Al, Al–Mg, and Al–Si Powders: Effect of Processing Conditions and Powder Properties," J. Mater. Process. Technol., **213**(8), pp. 1387–1405.
[30] DeGarmo, P. E., Black, J. T., and Kohser, R. A., 2003, *Materials and Processes in Manufacturing*, Wiley, Hoboken, NJ.